

RECEIVED: April 25, 2012

REVISED: June 25, 2012

ACCEPTED: July 6, 2012

PUBLISHED: July 20, 2012

# LHC and Tevatron bounds on the dark matter direct detection cross-section for vector mediators

**Mads T. Frandsen, Felix Kahlhoefer, Anthony Preston, Subir Sarkar  
and Kai Schmidt-Hoberg**

*Rudolf Peierls Centre for Theoretical Physics, University of Oxford,  
1 Keble Road, Oxford OX1 3NP, U.K.*

*E-mail:* [m.frandsen1@physics.ox.ac.uk](mailto:m.frandsen1@physics.ox.ac.uk),  
[felix.kahlhoefer@physics.ox.ac.uk](mailto:felix.kahlhoefer@physics.ox.ac.uk), [a.preston1@physics.ox.ac.uk](mailto:a.preston1@physics.ox.ac.uk),  
[s.sarkar@physics.ox.ac.uk](mailto:s.sarkar@physics.ox.ac.uk), [ksh@physics.ox.ac.uk](mailto:ksh@physics.ox.ac.uk)

**ABSTRACT:** We study the interactions of a new spin-1 mediator that connects the Standard Model to dark matter. We constrain its decay channels using monojet and monophoton searches, as well as searches for resonances in dijet, dilepton and diboson final states including those involving a possible Higgs. We then interpret the resulting limits as bounds on the cross-section for dark matter direct detection without the need to specify a particular model. For mediator masses between 300 and 1000 GeV these bounds are considerably stronger than the ones obtained under the assumption that the mediator can be integrated out.

**KEYWORDS:** Beyond Standard Model, Cosmology of Theories beyond the SM

**ARXIV EPRINT:** [1204.3839](https://arxiv.org/abs/1204.3839)

---

## Contents

<b>1</b>	<b>Introduction</b>	<b>1</b>
<b>2</b>	<b>Interactions of a neutral spin-1 mediator</b>	<b>3</b>
2.1	Effective Lagrangian description	3
2.2	Production and decay of $R$ at colliders	4
<b>3</b>	<b>Collider bounds</b>	<b>5</b>
3.1	Monojet searches	6
3.2	Monophoton searches	7
3.3	Dijet resonances	8
3.4	Top pairs	8
3.5	Dilepton resonances	9
3.6	$WW$ and $ZZ$	9
3.7	$ZH$	9
<b>4</b>	<b>Implications for dark matter direct detection</b>	<b>10</b>
4.1	Direct detection through direct couplings	11
4.2	Direct detection through mixing	13
<b>5</b>	<b>Discussion</b>	<b>15</b>
<b>A</b>	<b>Decay widths</b>	<b>17</b>
<b>B</b>	<b>Coupling structure from mixing</b>	<b>18</b>

---

## 1 Introduction

Although the Large Hadron Collider (LHC) has yet to see any evidence for physics beyond the Standard Model (SM), we know from astrophysical and cosmological observations that the SM is incomplete, because it lacks an adequate candidate for the dark matter (DM) particle. Moreover, there are likely to be new interactions that connect the DM particle to the SM. In this paper, we discuss how colliders — and especially the LHC — can contribute to the search for DM and such new interactions.

The search for dark matter has mainly been focused on particles with mass and interactions set by the Fermi scale, e.g. neutralinos in extensions of the SM with softly broken supersymmetry (SUSY) at this scale. With an impressive increase of sensitivity over the past few years, direct detection experiments such as XENON100 [1] and CDMS-II [2, 3] have pushed down upper bounds on the (spin-independent) scattering cross-section on nuclei for such particles and have begun to constrain the relevant SUSY parameter space.

For much lighter DM particles, however, direct detection bounds become significantly weaker and at the same time such particles must have stronger interactions if their relic annihilations are to result in an acceptable DM abundance. Hence an improvement of the bounds for light DM is of great interest especially since recent results from the DAMA [4], CoGeNT [5] and CRESST-II [6] experiments hint at DM with mass  $m_\chi \sim 10 \text{ GeV}$  and cross-section  $\sigma_p \sim 10^{-40} \text{ cm}^2$ . If DM does have such properties, then production of DM pairs at the LHC would be sizeable and result in a variety of observable signals.

Among the most promising signatures of DM at high energy colliders are excesses of events with either a single high-energy jet or a single high-energy photon and a large amount of missing transverse energy (MET). Such monojet and monophoton searches have been performed at LEP, Tevatron and the LHC but no excess has been observed over expected SM backgrounds [7–12]. If the mediator of the DM interaction with the SM is so heavy that it cannot be produced on-shell at the LHC, then these searches directly bound the coupling of DM to nucleons and are competitive with the bounds set by direct detection experiments [13–21]. However, for such large mediator masses, the relevant cross-sections for both the LHC and direct detection experiments will be very small unless the coupling constants approach the bounds from perturbative unitarity [18–20].

Of course the mediator mass may well be comparable to LHC energies. In this case an effective operator description is no longer valid, because the LHC can resolve the interaction and produce the mediator on-shell, which complicates the comparison with direct detection experiments. On the plus side, it opens up the possibility to search for resonances in various channels from the decays of the new mediator into SM particles. Combining the limits from all relevant collider searches, it is still possible to constrain the direct detection cross-section in a *model independent* way.

In particular, if DM is light compared to the dominant mediator, we can bound the DM direct detection cross-section in terms of the total width and the invisible branching ratio of the mediator in a simple way. These two quantities may in turn be constrained by collider searches without having to specify an underlying model — even though the collider bounds may be much stronger in a specific model framework. In this paper we apply this approach, assuming that the interaction between DM and the SM is dominated by the exchange of a neutral spin-1 state, here termed  $R$ . An example of such a spin-1 state is the  $Z'$  associated with a new broken  $U(1)$  symmetry [22–35]. Another example is a new resonance associated with a strongly interacting extension of the SM [36, 37], e.g. an analogue of the neutral isospin zero  $\omega$  resonance in QCD. Recently, there have been analyses of the ‘dark Higgs’ associated with the  $Z'$  [38] and LHC signatures of a baryonic  $Z'$  [39].

The outline of this paper is as follows: in section 2 we introduce an effective Lagrangian for the spin-1 state, discuss the decay channels and present the production cross-sections at LHC and the Tevatron. In section 3 we first summarize the resulting collider bounds from LHC and Tevatron on the various decay modes of  $R$ , before discussing the bound for each decay mode in more detail. In section 4, we compare our results to limits from direct detection on spin-independent and spin-dependent interactions. We do this both model independently and in the framework of a spin-1 state coupling to the SM via kinetic and mass mixing only, as discussed above. A discussion of all assumptions and their validity is

given in section 5 together with our conclusions. Appendices A and B provide, respectively, all relevant formulae for the partial decay widths and the coupling constants of  $R$ .

## 2 Interactions of a neutral spin-1 mediator

We start from an effective Lagrangian (similar to [28]) describing the interactions of the neutral spin-1 state  $R$  with the SM fields and the DM particle. We then discuss all possible decay channels and describe how they can be constrained by collider searches.

### 2.1 Effective Lagrangian description

We divide the Lagrangian into the couplings to DM, SM fermions, SM gauge bosons, the Higgs, and anything else

$$\mathcal{L}^R = \mathcal{L}_{\text{DM}}^R + \mathcal{L}_{f\bar{f}}^R + \mathcal{L}_{\text{gauge}}^R + \mathcal{L}_H^R + \mathcal{L}_X^R. \quad (2.1)$$

Depending on whether DM is a Dirac fermion  $\chi$  or complex (pseudo-)scalar  $\phi$ , we define  $\mathcal{L}_{\text{DM}}^R \equiv \mathcal{L}_\chi^R$  or  $\mathcal{L}_{\text{DM}}^R \equiv \mathcal{L}_\phi^R$  as appropriate, where

$$\mathcal{L}_\chi^R = R_\mu \bar{\chi} \gamma^\mu (g_{\chi R}^V - g_{\chi R}^A \gamma^5) \chi, \quad \mathcal{L}_\phi^R = g_{\phi R} R_\mu J_\phi^\mu \quad (2.2)$$

and  $J_\phi^\mu \equiv i(\phi^* \partial^\mu \phi - \phi \partial^\mu \phi^*)$ . We will not consider the  $CP$ -odd operator  $R^\mu \partial_\mu (\phi^* \phi)$  here (for a discussion see e.g. [40]).

The interactions of  $R$  with the SM fermions are described by

$$\mathcal{L}_{f\bar{f}}^R = \sum_{f=q,\ell,\nu} R_\mu \bar{f} \gamma^\mu (g_{fR}^V - g_{fR}^A \gamma^5) f, \quad (2.3)$$

where  $q, \ell, \nu$  denote SM quarks, charged leptons and neutrinos respectively.

Neglecting  $CP$ -violating terms (see e.g. [41] for a more complete discussion) the couplings of  $R$  to SM gauge fields can be written as

$$\begin{aligned} \mathcal{L}_{\text{gauge}}^R = & g_{WW1}^R [[RW^+W^-]]_1 + g_{WW2}^R [[RW^+W^-]]_2 \\ & + g_{ZW1}^R ((RZW^+W^-)) + g_{\gamma W1}^R ((R\gamma W^+W^-)) \\ & + g_{ZZ}^R [[RZZ]]_\epsilon + g_{Z\gamma}^R [[RZ\gamma]]_\epsilon + g_{WW3}^R [[RW^+W^-]]_\epsilon \\ & + g_{ZW2}^R \epsilon^{\mu\nu\rho\sigma} R_\mu Z_\nu W_\rho^+ W_\sigma^- + g_{\gamma W2}^R \epsilon^{\mu\nu\rho\sigma} R_\mu \gamma_\nu W_\rho^+ W_\sigma^-, \end{aligned} \quad (2.4)$$

where

$$\begin{aligned} [[RW^+W^-]]_1 &\equiv i [(\partial_\mu W_\nu^+ - \partial_\nu W_\mu^+) W^{\mu-} R^\nu - (\partial_\mu W_\nu^- - \partial_\nu W_\mu^-) W^{\mu+} R^\nu], \\ [[RW^+W^-]]_2 &\equiv \frac{i}{2} (\partial_\mu R_\nu - \partial_\nu R_\mu) (W^{\mu+} W^{\nu-} - W^{\mu-} W^{\nu+}), \\ [[RV_1 V_2]]_\epsilon &\equiv \epsilon^{\mu\nu\rho\sigma} (V_{1\mu} \partial_\rho V_{2\nu} - \partial_\rho V_{1\mu} V_{2\nu}) R_\sigma, \\ ((RVW^+W^-)) &\equiv 2R_\mu V^\mu W_\nu^- W^{\nu+} - R_\mu W^{\mu+} V_\nu W^{\nu-} - R_\mu W^{\mu-} V_\nu W^{\nu+}, \end{aligned}$$

for appropriate combinations of  $V_i = \{\gamma, Z, W^+, W^-\}$ . The operators in the first two lines of equation (2.4) conserve  $C$  and  $P$  separately, while the operators in the last two lines are  $CP$  even but  $P$  odd. If the underlying theory violates  $CP$ , then  $CP$  violating couplings are also possible [42]. In principle there could also be a coupling between the  $R$  and two photons, leading to the decay  $R \rightarrow \gamma^* \gamma$ .<sup>1</sup> Such a decay would however correspond to a non-renormalisable operator which — in order to have any observable effects — would imply additional new physics at rather low scales. We will not discuss such operators.

For comparable couplings the triboson final states are suppressed compared to the diboson ones due to smaller available phase-space. This is expected when  $R$  is a new gauge boson (for details see e.g. [43]). Consequently, we will neglect triboson decays of  $R$  in the following.<sup>2</sup>

Finally, couplings of  $R$  to the SM Higgs are of the form

$$\mathcal{L}_H^R = g_{ZH}^R R_\mu Z^\mu H + g_{ZHH}^R R_\mu Z^\mu H^2. \quad (2.5)$$

Again, we expect decays into  $ZHH$  to be significantly suppressed compared to decays into  $ZH$  so we neglect them in the following. A coupling of  $R$  to  $HH$  is absent because  $H$  is a real scalar and terms proportional to  $\partial_\mu R^\mu$  are  $CP$  violating hence we neglect them [41].

Leaving  $\mathcal{L}_X^R$  unspecified for now, the decay modes of the vector  $R$  may then be summarized as

$$\Gamma_R = \Gamma^{\chi\bar{\chi}} + \sum_q \Gamma^{q\bar{q}} + \sum_\ell \Gamma^{\ell\bar{\ell}} + \sum_\nu \Gamma^{\nu\bar{\nu}} + \Gamma^{WW} + \Gamma^{ZZ} + \Gamma^{\gamma Z} + \Gamma^{ZH} + \Gamma^X, \quad (2.6)$$

where the formulae for the partial widths are provided in appendix A. For consistency of our description, we will impose  $\Gamma_R/m_R < 1$  which already gives a bound on all coupling constants. If we define  $g_\psi \equiv \sqrt{(g_{\psi R}^V)^2 + (g_{\psi R}^A)^2}$  for any fermion  $\psi$  we then have the following constraints on the couplings in isolation

$$g_{\phi R} \lesssim 12, \quad g_\chi \lesssim 6, \quad g_\ell, g_\nu \lesssim 3.5, \quad g_q \lesssim 1.5. \quad (2.7)$$

Here we assumed family-independent SM couplings:  $g_u = g_d \equiv g_q$ .

## 2.2 Production and decay of $R$ at colliders

At colliders, the new spin-1 state  $R$  can e.g. be produced via Drell-Yan (DY) production, vector boson fusion (VBF) or ‘ $R$ -Strahlung’ from a SM gauge boson. We will focus in this paper on DY production. However, VBF will be important if the coupling of  $R$  to  $W$ ’s is large, e.g. if  $R$  arises from a composite theory. In this case, there would be more search channels with 2 additional jets in the final state.

In the case of DY production, we can decompose the cross-section for the production of  $R$  in association with an additional particle  $Y$  and subsequent decay of  $R$  into  $xy$ , as

$$\sigma(q\bar{q} \rightarrow R + Y \rightarrow xy + Y) = \sigma(q\bar{q} \rightarrow R + Y) \cdot \text{BR}(R \rightarrow xy), \quad (2.8)$$

<sup>1</sup>Note that the Landau-Yang theorem only applies to on-shell photons.

<sup>2</sup>However if  $R$  is a ‘techni-omega’, the coupling to the triboson final states can be enhanced so that the corresponding decays contribute significantly to the total width of  $R$ .

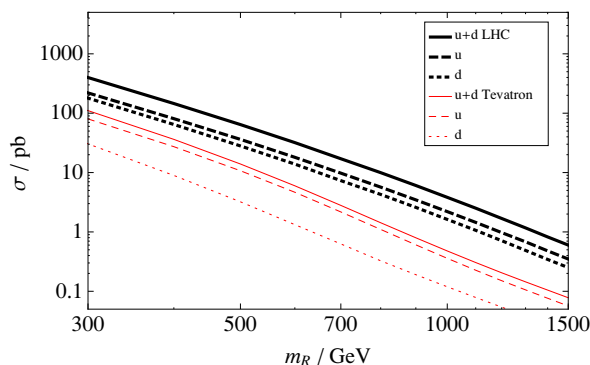


**Figure 1.** Drell-Yan production of  $R$  as a function of  $m_R$  at the LHC (with  $\sqrt{s} = 7$  TeV) and at the Tevatron for  $g_{u,d}^{A,V}$  equal to those of the SM  $Z$  boson (solid lines). We also show the production cross-section for the case that  $R$  couples either only to  $u$ -quarks or only to  $d$ -quarks.

where we have used the narrow width approximation (NWA), applicable if  $\Gamma_R/m_R \ll 1$ .

As a consequence of the NWA, the DY cross-section  $\sigma(q\bar{q} \rightarrow R \rightarrow xy)$  can be written as [44, 45]

$$\sigma_{xy} \propto [g_u^2 w_u(s, m_R^2) + g_d^2 w_d(s, m_R^2)] \cdot \text{BR}(R \rightarrow xy), \quad (2.9)$$

where  $w_{u,d}$  parameterise the parton distribution functions (PDFs) of the proton. For a narrow resonance the only dependence of the  $w_{u,d}$  coefficient on the resonance  $R$  is through  $m_R$ . Since the functions  $w_{u,d}$  are known, one can always translate a bound on  $g_u$  into a bound on  $g_d$  or a bound on a model with a given ratio of  $g_u/g_d$  into a bound on a different model. For this reason, we will show experimental bounds assuming  $g_u = g_d \equiv g_q$  for simplicity.

In figure 1 we show the leading order (LO) cross-section for  $\sigma(pp \rightarrow R)$ , with the couplings of  $R$  to SM fields set equal to those of the SM  $Z$  boson as well as the individual contributions from  $u$ -quarks and  $d$ -quarks. The production cross-section of  $R$  with different couplings may be found by a simple rescaling. Note that QCD corrections can enhance the DY production significantly; in the following, we take the K-factors from [45] for the MSTW08 NNLO PDF.

Once we know the production cross-section of  $R$  for given couplings  $g_q$ , we can translate LHC bounds on the cross-section for a certain final state  $xy$  into a bound on the product  $g_q^2 \cdot \text{BR}(R \rightarrow xy)$ . The decay modes of  $R$  into the  $X$  sector can appear at colliders as additional missing energy, displaced vertices or high-multiplicity SM final states. An example is the decay mode  $R \rightarrow Zh'$  where  $h'$  is a new scalar state responsible for the mass of  $R$ . Another contribution to  $\Gamma^X$  could come from decay modes of  $R$  to additional hidden sector states. A number of such possibilities were considered e.g. in [46].

### 3 Collider bounds

In this section we summarize the collider bounds from LHC and Tevatron for the decay modes of  $R$  and then discuss each decay mode in more detail. Table 1 lists the current

Channel [Exp]	L [fb <sup>-1</sup> ]	Mass range	Couplings	Reference
$pp \rightarrow j + \cancel{p}_T$ [ATLAS]	1.0	*	$g_q g_\chi$	[10]
$pp \rightarrow j + \cancel{p}_T$ [CMS]	4.7	*	$g_q g_\chi$	[9]
$pp \rightarrow j + \cancel{p}_T$ [CDF]	6.7	*	$g_q g_\chi$	[8]
$pp \rightarrow \gamma + \cancel{p}_T$ [CMS]	1.14	*	$g_q g_\chi, g_q g_{Z\gamma}^R$	[11]
$pp \rightarrow \gamma + \cancel{p}_T$ [CMS]	4.7	*	$g_q g_\chi, g_q g_{Z\gamma}^R$	[12]
$pp \rightarrow j j$ [ATLAS]	1.04	900 – 4000	$g_q$	[47]
$pp \rightarrow j j$ [CDF]	1.13	250 – 1400	$g_q$	[48]
$pp \rightarrow \ell \ell$ [CMS]	4.9	300 – 2500	$g_q g_\ell$	[49]
$pp \rightarrow \ell \ell$ [ATLAS]	1.08–1.21	200 – 2000	$g_q g_\ell$	[50]
$pp \rightarrow \tau \tau$ [CMS]	4.9	350 – 1600	$g_q g_\tau$	[51]
$pp \rightarrow Z Z^{(*)}$ [ATLAS]	4.9	110 – 600	$g_q g_{ZZ}^R$	[52]
$pp \rightarrow Z Z$ [ATLAS]	1.0	320 – 1500	$g_q g_{ZZ}^R$	[53]
$pp \rightarrow Z Z^{(*)}$ [CMS]	4.6 – 4.8	110 – 600	$g_q g_{ZZ}^R$	[54]
$pp \rightarrow W W^{(*)}$ [ATLAS]	4.9	110 – 600	$g_q g_{WW}^R$	[52]
$pp \rightarrow W W^{(*)}$ [CMS]	4.6 – 4.8	110 – 600	$g_q g_{WW}^R$	[54]
$pp \rightarrow ZH$ [ATLAS]	4.7	*	$g_q g_{ZH}^R$	[55]
$pp \rightarrow t \bar{t}$ (boosted) [CMS]	4.6	1000 – 3000	$g_q g_t$	[56]
$pp \rightarrow t \bar{t}$ (semileptonic) [CMS]	4.9	500 – 1500	$g_q g_t$	[57]

**Table 1.** Collider searches in final states that constrain the couplings of  $R$ . Fields marked with a \* correspond to searches that do not look for heavy resonances and which, consequently, give constraints for arbitrary  $m_R$ . In the case of scalar DM  $g_\chi$  should be replaced by  $g_{\phi R}$ .

collider searches we consider here, while the corresponding limits we derive are summarised in figure 2 and figure 3. The confidence level for all bounds is at least 95%.

### 3.1 Monojet searches

The monojet final state arises from production of  $R$  with an additional jet,  $j = q, g$ , followed by the decay of  $R$  into DM or neutrinos:  $\sigma(pp \rightarrow jR \rightarrow j \cancel{p}_T)$ . Decay modes into additional hidden sector states also contribute to the monojet signal, provided these states do not decay back to SM states within the detector.

Monojet searches have been performed at the Tevatron [8, 58], and at the LHC by both CMS [9] and ATLAS [59] with similar sensitivity. To calculate our bounds we compare the limits from ATLAS with the parton-level monojet signal from  $R$  simulated using CalcHEP [60]. For monojet searches, the jets have sufficiently high  $p_T$  that the errors from neglecting parton showering and hadronization are small (see e.g. [14, 61]).

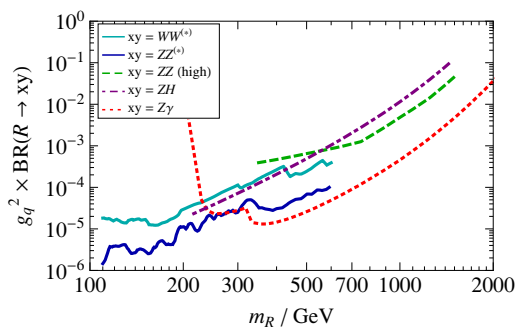


**Figure 2.** Bounds on  $g_q^2 \cdot \text{BR}(R \rightarrow xy)$  as a function of  $m_R$ , with  $xy$  being either SM gauge bosons or  $ZH$ .

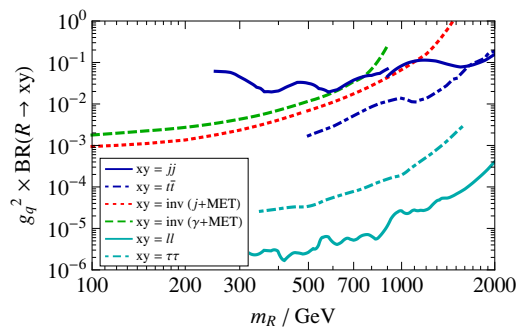


**Figure 3.** Bounds on  $g_q^2 \cdot \text{BR}(R \rightarrow xy)$  as a function of  $m_R$ , with  $xy$  being either SM fermions or DM particles.

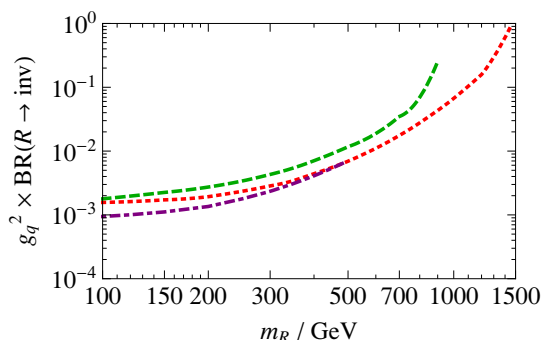


**Figure 4.** Limits on  $g_q^2 \cdot \text{BR}(R \rightarrow \text{inv})$  from monojet searches (red, dotted and purple, dot-dashed) [10] and the monophoton searches (green, dashed) [12]. The red dotted line corresponds to the cut  $p_T > 350$  GeV, the purple dot-dashed line to  $p_T > 250$  GeV.

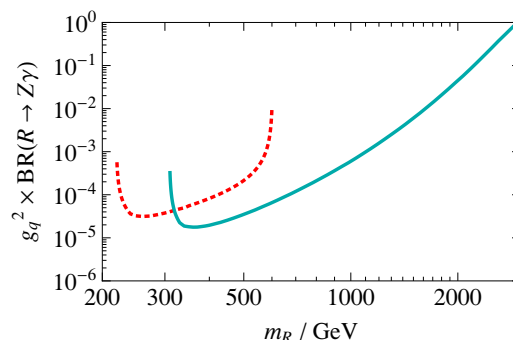


**Figure 5.** Limits on  $g_q^2 \cdot \text{BR}(R \rightarrow Z\gamma)$  from the monophoton searches in ref. [11] (red, dotted) and ref. [12] (light blue, solid).

For  $m_R \gtrsim 400$  GeV, we find that the ATLAS search with  $p_T(j) > 350$  GeV gives the strongest constraint. For lighter  $R$ , a stronger bound is obtained from the ATLAS search with  $p_T(j) > 250$  GeV. The Tevatron gives the strongest bound for  $m_R \lesssim 100$  GeV because of its high luminosity and lower monojet  $p_T$  cut. Our results are shown in figure 4.

### 3.2 Monophoton searches

The monophoton final state can arise from two different processes. The first is similar to the monojet process with production of  $R$  and initial state radiation of a photon, followed by decay of  $R$  into DM or neutrinos  $\sigma(pp \rightarrow \gamma R \rightarrow \gamma \cancel{p}_T)$ . The second possibility is DY production of  $R$  followed by the direct decay of  $R$  into  $Z\gamma$ , with subsequent decay of  $Z$  to neutrinos  $\sigma(pp \rightarrow R \rightarrow \gamma Z \rightarrow \gamma \nu \bar{\nu})$ .

We find that the initial state radiation of a photon provides weaker constraints on the invisible branching ratio of  $R$  than the initial state radiation of a jet (see figure 4). The second process, however, offers an interesting possibility to limit the branching ratio of  $R \rightarrow Z\gamma$ . Note, however, that such monophoton searches are only sensitive to these



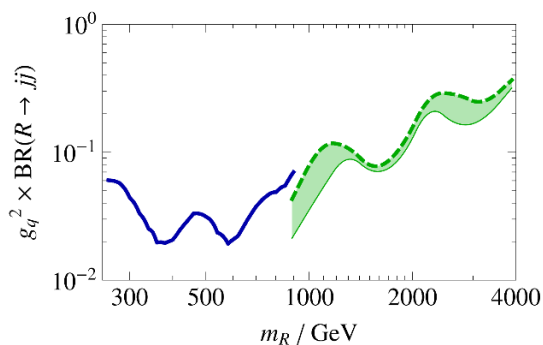


**Figure 6.** Combined dijet limits from CDF (blue, solid) and ATLAS (green, dashed). The line width reflects the dependence of the ATLAS bound on  $\Gamma_R$  (which is varied between 10% and 25% of the mediator mass).

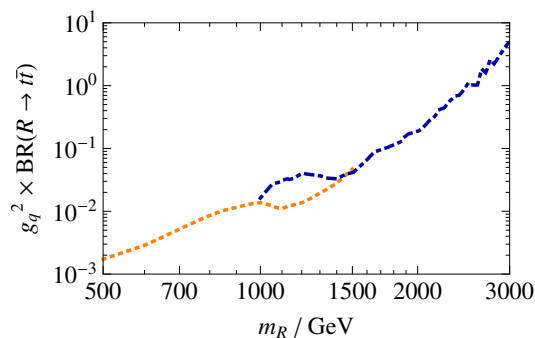


**Figure 7.** Limit on  $g_q^2 \cdot \text{BR}(R \rightarrow t\bar{t})$  from searches for boosted tops (blue, dot-dashed) [56] and semileptonic tops (orange, dotted) [57].

decays if  $m_R/2$  is sufficiently larger than any cut on  $\cancel{p}_T$  or the photon  $p_T$ . We use the data from [11, 12] and obtain the limit curves shown in figure 5 using **CalcHEP**. Note that the limits on the direct decay  $R \rightarrow Z\gamma$  have been calculated without including the contribution of invisible decays of  $R$  together with a photon (from initial state radiation). For sizeable invisible branching of  $R$ , the bounds would become even stronger.

### 3.3 Dijet resonances

Searches for resonances in the invariant mass distribution of dijet events have been carried out at Tevatron and at the LHC. We use the CDF limit [48] for  $m_R < 900$  GeV and the ATLAS limits [47] for  $m_R \geq 900$  GeV. In the latter case, the bound on the cross-section is not quite independent of the width of the resonance, which depends on  $\Gamma_R$  and on the detector resolution (see also [61]).

To estimate this dependence we have generated  $m_{jj}$  distributions for different values of  $\Gamma_R$  using **LanHEP** [62] and **CalcHEP** and convoluted these distributions with the detector resolution [47]. By comparing the resulting width of the peak to the bounds given in table II of [47] we estimate how the limit varies with the mediator width for  $\Gamma_R/m_R$  in the range 0.1–0.25. The result is shown in figure 6 together with the limits from dijet searches from CDF. We take the upper end of the band shown in figure 6 and conservatively apply it as a bound for all widths  $\Gamma_R/m_R < 0.25$ .

### 3.4 Top pairs

Searches for dijet resonances constrain the decays of  $R$  into the five lightest quarks. To constrain  $g_q^2 \cdot \text{BR}(R \rightarrow t\bar{t})$  independently, we use the dedicated CMS searches [56, 57] for  $t\bar{t}$  resonances. The resulting bounds are shown in figure 7.

We note that for family independent couplings and assuming  $m_R > 2m_t$ , we can always use a bound on  $g_q^2 \cdot \text{BR}(R \rightarrow jj)$  to infer a bound on  $g_q^2 \cdot \text{BR}(R \rightarrow t\bar{t})$  using the relation

$$\text{BR}(R \rightarrow t\bar{t}) = \frac{\sqrt{1 - 4m_t^2/m_R^2}}{2 + 3g_d^2/g_u^2} \cdot \text{BR}(R \rightarrow jj) . \quad (3.1)$$

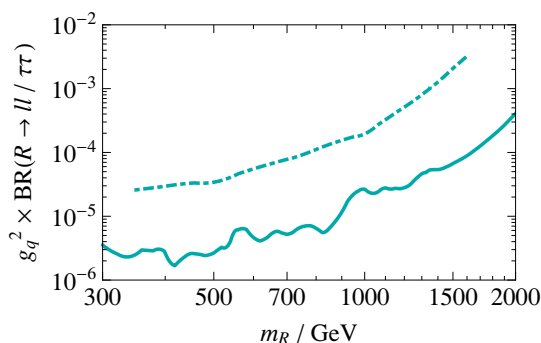


**Figure 8.** Limit on  $g_q^2 \cdot \text{BR}(R \rightarrow \ell\ell)$  (solid) from the CMS search for dilepton resonances [49] and on  $g_q^2 \cdot \text{BR}(R \rightarrow \tau\tau)$  (dotted) from the corresponding ditau search [51].

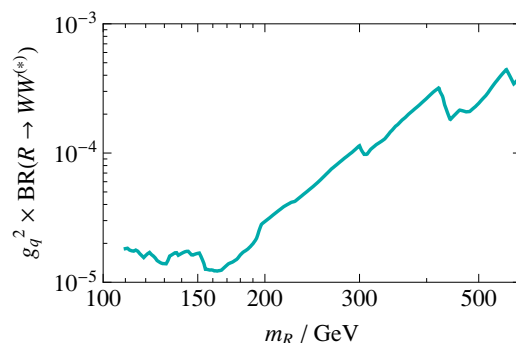


**Figure 9.** Limit on  $g_q^2 \cdot \text{BR}(R \rightarrow WW)$  from combined searches for Higgs decays to  $WW$  [52].

For  $g_u \sim g_d$ , the bound on  $g_q^2 \cdot \text{BR}(R \rightarrow t\bar{t})$  inferred from the dijet limit is comparable to the direct bound from top pair searches. As expected, for  $g_u \ll g_d$ , the inferred bound on  $g_q^2 \cdot \text{BR}(R \rightarrow t\bar{t})$  is much stronger than the direct one, while for  $g_u \gg g_d$ , we can actually invert the equation above to obtain a bound on  $g_q^2 \cdot \text{BR}(R \rightarrow jj)$  from the bounds on  $g_q^2 \cdot \text{BR}(R \rightarrow t\bar{t})$ .

### 3.5 Dilepton resonances

We consider the recent CMS search for dilepton resonances [49] with  $\ell = (e, \mu)$  as well as the search for ditau resonances [51] and show the resulting limits in figure 8. If we assume family independent couplings, we can obtain a stronger bound on the ditau channel making use of the relation  $\text{BR}(\tau\tau) = \text{BR}(\ell\ell)/2$ .

### 3.6 WW and ZZ

Searches for  $WW$  and  $ZZ$  final state have been performed in the context of Higgs searches at the LHC [52, 54] and as a dedicated search for high-mass resonances [53]. The results of these searches are shown in figures 9 and 10. We observe that the Higgs search limits from  $WW$  and  $ZZ$  on the  $R$  couplings are significant even for relatively large  $m_R$ . The reason is that for a vector boson, the coupling involves a derivative, so it is enhanced compared to e.g. the SM Higgs coupling for large masses.

### 3.7 ZH

Recent results from the LHC exclude the SM Higgs with a mass between 130 and 550 GeV at the 99% confidence level [52, 54], while the combined LEP2 results exclude it below 114.5 GeV at the 95% confidence level [63]. In the allowed mass range, we have upper limits on the cross-section  $pp \rightarrow ZH$  from searches for Higgs production in association with a SM vector. We take the limit from  $pp \rightarrow ZH \rightarrow \nu\bar{\nu}b\bar{b}$  from [55], giving  $\sigma_{ZH} < 1.7 \dots 2.0$  pb depending on the value of the Higgs mass in the allowed range. We show the resulting limit for  $m_H = 125$  GeV in figure 11.

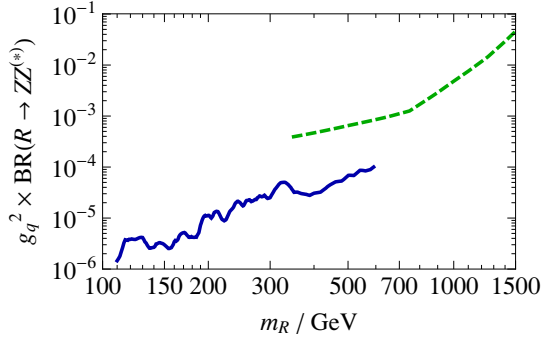


**Figure 10.** Limit on  $g_q^2 \cdot \text{BR}(R \rightarrow ZZ)$  from combined searches for Higgs decays to  $ZZ$  [52] (blue, solid) and from a dedicated search for high-mass  $ZZ$  resonances [53] (green, dashed).

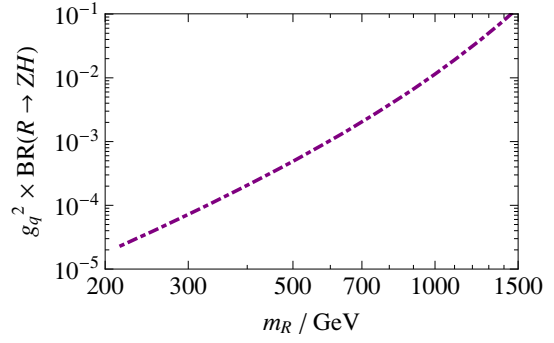


**Figure 11.** Limit on  $g_q^2 \cdot \text{BR}(R \rightarrow ZH)$  from the ATLAS search for associate production of Higgs and  $Z$  for a Higgs mass of  $m_H = 125$  GeV [55].

#### 4 Implications for dark matter direct detection

In this section, we apply the collider bounds obtained above to constrain DM-nucleon interactions mediated by  $R$ . We can calculate the direct detection cross-section by integrating out both  $R$  and  $Z$  to generate the corresponding effective operators. In the case of Dirac DM we obtain

$$\mathcal{L}_\chi^{\text{eff}} = b_f^V \bar{\chi} \gamma_\mu \chi \bar{f} \gamma^\mu f + b_f^A \bar{\chi} \gamma_\mu \gamma^5 \chi \bar{f} \gamma^\mu \gamma^5 f, \quad (4.1)$$

where we have neglected terms that vanish in the non-relativistic limit and defined the effective couplings

$$b_f^{A,V} = b_{fR}^{A,V} + b_{fZ}^{A,V} = \frac{g_{\chi R}^{A,V} g_{fR}^{A,V}}{m_R^2} + \frac{g_{\chi Z}^{A,V} g_{fZ}^{A,V}}{m_Z^2}. \quad (4.2)$$

Unless  $b^V$  is very small compared to  $b^A$ , the direct detection cross-section will be dominated by the effective vector-vector interaction between the DM particle and nucleons ( $p, n$ ) given by

$$\mathcal{L}_\chi^V = f_p^X \bar{\chi} \gamma_\mu \chi \bar{p} \gamma^\mu p + f_n^X \bar{\chi} \gamma_\mu \chi \bar{n} \gamma^\mu n; \quad f_p^X = 2b_u^V + b_d^V, \quad f_n^X = 2b_d^V + b_u^V. \quad (4.3)$$

In the case of the complex scalar DM we have, similarly,

$$\mathcal{L}_\phi^{\text{eff}} = a_f^V J_\phi^\mu \bar{f} \gamma_\mu f, \quad \mathcal{L}_\phi^V = f_p^\phi J_\phi^\mu \bar{p} \gamma_\mu p + f_n^\phi J_\phi^\mu \bar{n} \gamma_\mu n, \quad (4.4)$$

where

$$a_f^V = a_{fR}^V + a_{fZ}^V = \frac{g_{\phi R} g_{fR}^V}{m_R^2} + \frac{g_{\phi Z} g_{fZ}^V}{m_Z^2}; \quad f_p^\phi = 2a_u^V + a_d^V, \quad f_n^\phi = 2a_d^V + a_u^V. \quad (4.5)$$

Because of the conservation of the vector current, there is no contribution of sea quarks or gluons to the effective couplings. For both Dirac and complex scalar DM we obtain the DM-nucleon cross-section

$$\sigma_N = \mu_{\chi N}^2 f_N^2 / \pi, \quad \text{where } N = p, n. \quad (4.6)$$

In the following, we will consider two different possibilities for generating effective interactions of nucleons and DM particles. First we consider the case where  $R$  has sizeable direct couplings to quarks and all other couplings are arbitrary. Afterwards we consider the case where the interaction state  $X$  corresponding to the mass eigenstate  $R$  couples only to the DM particle and couplings to SM particles are generated only via mixing. An example would be the ‘dark’  $Z'$ , where  $R$  is the gauge boson of a new  $U(1)$  under which only the DM particle is charged. In this case, we can use collider bounds to directly constrain the mixing parameters, and therefore the direct detection cross-section.

#### 4.1 Direct detection through direct couplings

Let us start with the general case where  $R$  can have arbitrary couplings to SM particles. The only assumption we make is that  $R$  has a sizeable branching into quarks. This assumption is important for two reasons. First, we want to exclude the case where  $g_q$  is so small that the total number of  $R$ -particles produced at the LHC is insufficient to give a detectable monojet signal. We will come back to the case where  $g_\chi \gg g_{uR}^V, g_{dR}^V$  in section 4.2.

Second, this assumption ensures that DM direct detection is dominated by  $R$ -exchange, with  $Z$ -exchange giving only a negligible contribution. This case is interesting because it allows a ratio  $f_n/f_p$  significantly different from the one for  $Z$  exchange. In fact defining  $y \equiv g_{uR}^V/g_{dR}^V$  we obtain  $f_n/f_p = (y+2)/(2y+1)$ , which can in principle take any arbitrary value.

We then obtain from equation (4.6)

$$\sigma_p \simeq (2y+1)^2 \frac{\mu_{\chi n}^2}{\pi} \frac{(g_{dR}^V)^2 (g_{\chi R}^V)^2}{m_R^4} \leq (2y+1)^2 \frac{\mu_{\chi n}^2}{\pi} \frac{g_d^2 g_\chi^2}{m_R^4}. \quad (4.7)$$

For  $m_\chi \ll m_R$  we can use equation (A.1) to obtain

$$\sigma_p \leq 12(2y+1)^2 \frac{\mu_{\chi n}^2 \Gamma_R}{m_R^5} g_d^2 \cdot \text{BR}(R \rightarrow \text{inv}). \quad (4.8)$$

As discussed in section 3, monojet and monophoton searches at the LHC provide a limit on  $g_d^2 \cdot \text{BR}(R \rightarrow \text{inv})$ , so that we obtain a bound on the direct detection cross-section if we can constrain  $\Gamma_R$ .

Of course, if we allow decays into new states that give complicated experimental signatures, we can make  $\Gamma_R$  arbitrarily large. Therefore, we will now assume that all new states are either SM particles, or remain invisible, i.e. escape the detector without decaying into visible particles. In that case, we can combine the bounds from section 3 to obtain an upper limit on  $g_d$  and, assuming family independent couplings, constrain  $\Gamma_R$ . The resulting bounds are shown in figures 12 and 13.

With present data, we can constrain  $g_d$  and  $\Gamma_R$  only in the range  $300 \text{ GeV} \leq m_R \leq 600 \text{ GeV}$ . However, the only decay channel that is presently not available above 600 GeV is  $R \rightarrow WW$ . We simply assume that upcoming searches for this decay mode will give bounds comparable to the current bounds for  $R \rightarrow ZZ$ . Consequently, we assume that the bound on  $g_q^2 \cdot \text{BR}(R \rightarrow ZZ)$  also applies to  $g_q^2 \cdot \text{BR}(R \rightarrow WW)$  so that we can extend our analysis up to 1200 GeV. Even a somewhat weaker bound on  $g_q^2 \cdot \text{BR}(R \rightarrow WW)$  would

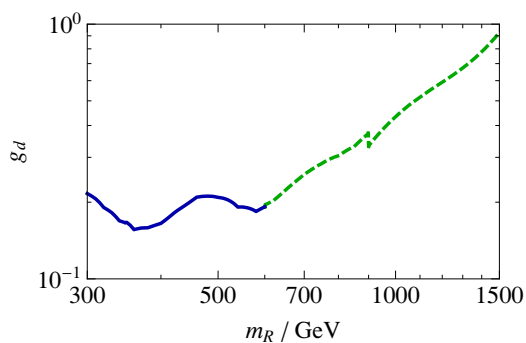


**Figure 12.** Limit on  $g_d$  from the combination of all experimental bounds (see text).

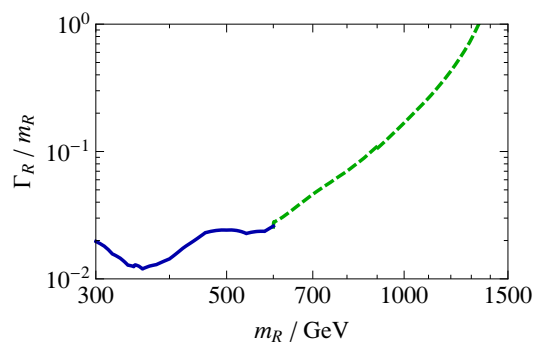


**Figure 13.** Limit on  $\Gamma_R$  from the combination of all experimental bounds.

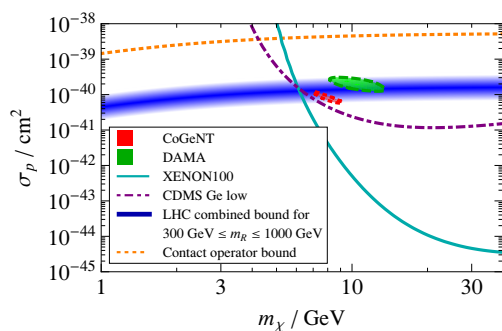
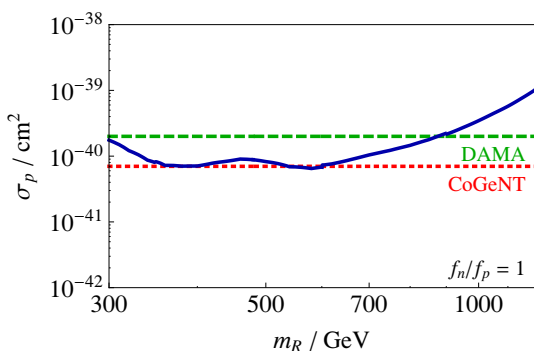


**Figure 14.** Left: bound from LHC data on the direct detection cross-section as a function of the mediator mass  $m_R$  with the DM mass  $m_\chi = 10$  GeV. Right: bound on the direct detection cross-section from LHC limits as a function of the DM mass  $m_\chi$  compared to the results from various direct detection experiments. The width of the blue line corresponds to the change of the bound as the mediator mass is varied between 300 and 1000 GeV. For larger or smaller mediator masses, the bound would become weaker. As an example, we show the bound obtained from the contact operator if the mediator can be integrated out [18].

not change our results dramatically, because decays into  $WW$  give only a subdominant contribution to the total width of  $R$ .

We observe that up to  $m_R \sim 1000$  GeV,  $\Gamma_R/m_R$  remains sufficiently small that the NWA stays valid, which is an important consistency requirement for our treatment. We can therefore use the limit on  $\Gamma_R$  from figure 13 to calculate an upper bound on the direct detection cross-section. The resulting bounds on the direct detection cross-section both as a function of mediator mass and as a function of DM mass are shown in figure 14. We observe that we can exclude a cross-section of  $\sigma_p = 2 \times 10^{-40} \text{cm}^2$  over the full mass range  $300 \text{ GeV} \leq m_R \lesssim 1000 \text{ GeV}$ , as long as  $m_\chi \ll m_R$ .

So far, we have only considered standard spin-independent interactions of DM. Many other possibilities have been considered in the literature, e.g. spin-dependent interactions, momentum-dependent interactions, inelastic DM, and effective couplings with  $f_n \neq f_p$  (see e.g. [64]). Typically, these interactions strongly suppress scattering in the non-relativistic limit, while the results from LHC searches are not significantly affected. As a result, the

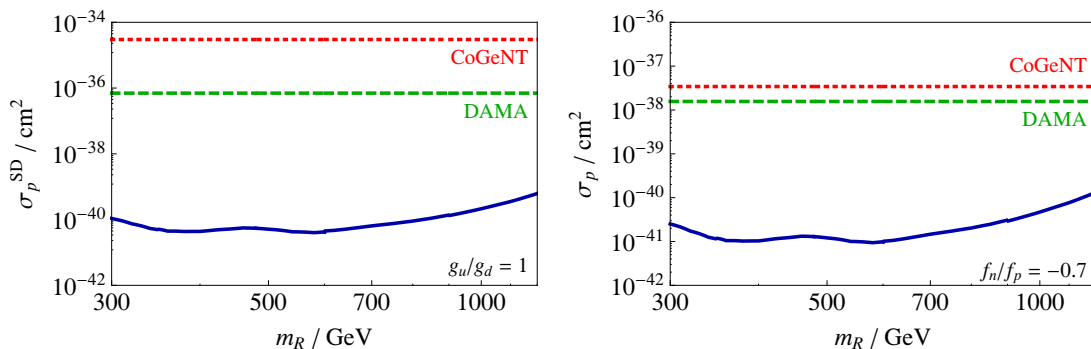


**Figure 15.** Left: bound on the spin-dependent direct detection cross-section from LHC limits as a function of the mediator mass  $m_R$  with the DM mass fixed to  $m_\chi = 10$  GeV. Right: same but for spin-independent interactions with the isospin-violating couplings  $f_n/f_p = -0.7$ .

LHC bounds will become much stronger compared to any exclusion limits (or claimed signals) from direct detection experiments. To illustrate this point, we show in figure 15 the LHC bounds for spin-dependent interactions, as well as spin-independent interactions with  $f_n/f_p = -0.7$ .

To conclude this section, we discuss how our results would change for complex scalar DM (e.g. a scalar technibaryon [36, 37, 65, 66]). In fact, all the experimental limits can be applied in complete analogy, the only difference being that for identical couplings the partial width for decays into scalar DM is smaller by a factor of 4, cf. appendix A. As a consequence, the bounds on the direct detection cross-section will be *weaker* by a factor of 4, excluding  $\sigma_p > 8 \times 10^{-40}$  cm<sup>2</sup> for  $m_\chi \ll m_R$  and  $300 \text{ GeV} < m_R < 1000 \text{ GeV}$ .

## 4.2 Direct detection through mixing

Now we consider the case where  $R$  is the mass eigenstate that corresponds to the gauge boson  $X$  of a new  $U(1)_X$  gauge group.  $X$  is then described by an effective Lagrangian, which includes kinetic mixing and mass mixing (see also appendix B)

$$\begin{aligned} \mathcal{L} = \mathcal{L}_{SM} &- \frac{1}{4} \hat{X}^{\mu\nu} \hat{X}_{\mu\nu} + \frac{1}{2} m_X^2 \hat{X}_\mu \hat{X}^\mu - m_\chi \bar{\chi} \chi \\ &- \frac{1}{2} \sin \epsilon \hat{B}_{\mu\nu} \hat{X}^{\mu\nu} + \delta m^2 \hat{Z}_\mu \hat{X}^\mu - f_\chi^V \hat{X}^\mu \bar{\chi} \gamma_\mu \chi. \end{aligned} \quad (4.9)$$

We assume that the interaction eigenstate  $X$  couples only to the DM particle  $\chi$  (assumed here to be a Dirac fermion) with strength  $f_\chi^V$ , and has no other couplings. In particular, we assume that other hidden sector states — even if present — give a negligible contribution to the total width of  $R$ .

The mass eigenstate  $R$  then picks up SM couplings from mixing as described in appendix B. At the same time, kinetic mixing introduces a coupling between  $\chi$  and the  $Z$ -boson. After integrating out both  $R$  and  $Z$ , the resulting coupling constants for the effective interactions between DM and nucleons are, in terms of the Lagrangian parameters

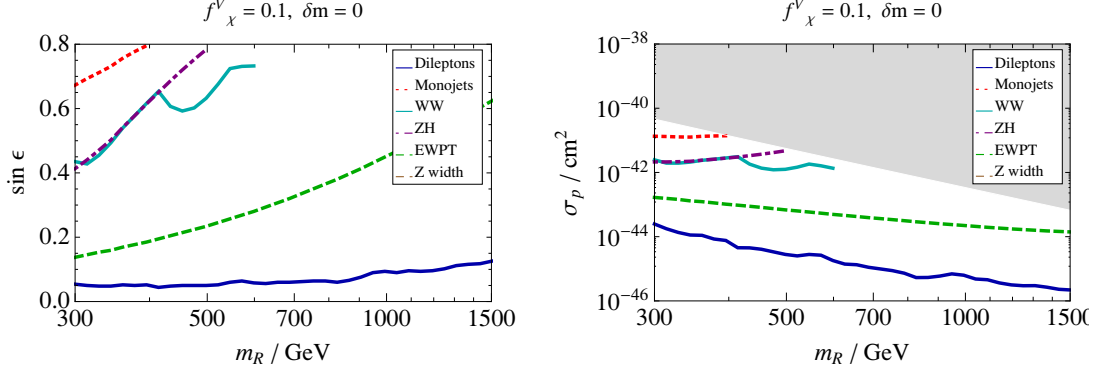


**Figure 16.** Bounds on the mixing parameter  $\sin \epsilon$  and the direct detection cross-section  $\sigma_p$  for  $f_\chi^V = 0.1$  and  $\delta m = 0$ . The grey shaded region in the second plot corresponds to  $\sin \epsilon > 0.8$ .

in equation (4.9)

$$\begin{aligned}
 f_p &= \frac{\hat{g} f_\chi^V}{4\hat{c}_W} \frac{c_\xi^2}{c_\epsilon} t_\xi \left[ (1 - 4\hat{s}_W^2 - 3\hat{s}_W t_\epsilon t_\xi) \frac{1}{m_Z^2} - \left( 1 - 4\hat{s}_W^2 + 3\hat{s}_W \frac{t_\epsilon}{t_\xi} \right) \frac{1}{m_R^2} \right], \\
 f_n &= -\frac{\hat{g} f_\chi^V}{4\hat{c}_W} \frac{c_\xi^2}{c_\epsilon} t_\xi \left[ (1 + \hat{s}_W t_\epsilon t_\xi) \frac{1}{m_Z^2} - \left( 1 - \hat{s}_W \frac{t_\epsilon}{t_\xi} \right) \frac{1}{m_R^2} \right],
 \end{aligned} \tag{4.10}$$

where  $\xi$  is defined in equation (B.9) and we abbreviated  $\sin \theta \equiv s_\theta$ ,  $\cos \theta \equiv c_\theta$ ,  $\tan \theta \equiv t_\theta$ . In the case where the mass mixing parameter  $\delta m = 0$ , we obtain  $f_n \simeq 0$ , i.e. photon-like interactions.

Because of mixing  $R$  can be produced directly in  $p$ - $p$  collisions, so we can use LHC data to constrain the mixing parameters and therefore obtain bounds on the direct detection cross-section. In addition to the LHC bounds, we also have LEP bounds on the kinetic mixing parameters  $\sin \epsilon$  and  $\xi$  and on  $g_{\chi Z}$ . In order to satisfy electroweak precision tests (EWPT) we must require that [23]

$$\alpha S = 4\xi \hat{c}_W^2 \hat{s}_W t_\epsilon, \quad \text{and} \tag{4.11}$$

$$\alpha T = \xi^2 (m_{\hat{X}}^2 / m_Z^2 - 1) + 2\xi \hat{s}_W t_\epsilon, \tag{4.12}$$

are within their experimental limits. Moreover, from measurements of the  $Z$  invisible width, we know that

$$(g_{\chi Z})^2 \lesssim 0.008. \tag{4.13}$$

Note, however, that new physics might well give additional contributions to the  $S$  and  $T$  parameters, which can modify these bounds.

For fixed  $f_\chi^V$  and  $\delta m$  we can calculate all coupling constants and therefore the partial decay widths and branching ratios of  $R$  as a function of  $m_R$  and  $\sin \epsilon$ . The bounds from section 3 can then be interpreted as constraints on  $\sin \epsilon$  as a function of  $m_R$ . These constraints directly correspond to limits on the DM direct detection cross-section. Our results are presented in figure 16.

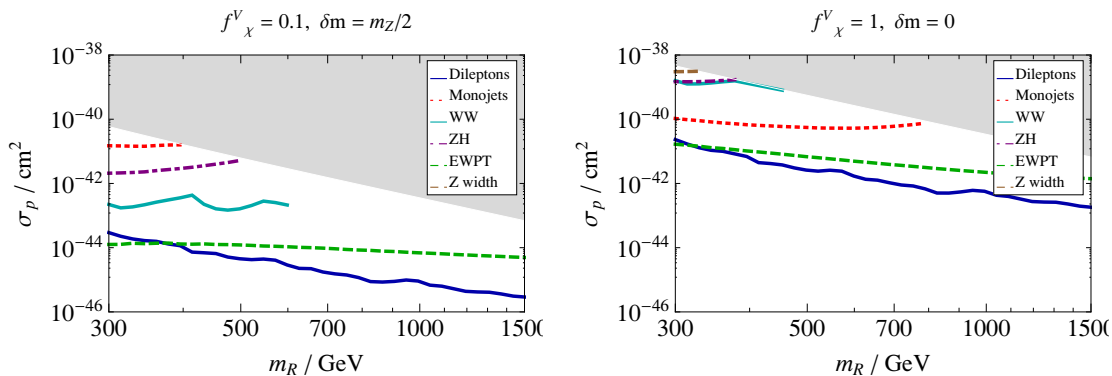


**Figure 17.** Bounds on the direct detection cross-section for different choices of  $f_\chi^V$  and  $\delta m$ . The grey shaded regions correspond to  $\sin \epsilon > 0.8$ .

We observe that the bound from  $WW$  does not get stronger compared to the other bounds as we increase  $m_R$ , despite the enhancement of the branching ratio of  $R$  into  $WW$ . The reason is that for small kinetic mixing, the coupling of  $R$  to quarks and leptons is proportional to  $\cos \xi t_\epsilon \approx \epsilon$ , while the coupling of  $R$  to  $WW$  is proportional to  $\sin \xi \approx \epsilon \sin \theta_W M_Z^2 / m_R^2$ . Thus, the partial width  $\Gamma^{WW}$  picks up an additional factor of  $m_Z^4 / m_R^4$  which precisely cancels the enhancement from the derivative interaction.

In the case where  $f_\chi^V = 0.1$ , the LHC gives strong constraints on the direct detection cross-section, comparable to the best bounds from current direct detection experiments. This conclusion does not change significantly, if we include a mass mixing term (see figure 17). However, such a mass mixing will enhance  $\xi$  compared to  $\epsilon$ , so the bound from  $WW$  becomes stronger compared to the bound from dileptons and monojets.

Increasing  $f_\chi^V$  relaxes all bounds from the LHC since smaller quark couplings, and therefore smaller mixing parameters are required for the same direct detection cross-section. At the same time the invisible partial width of  $R$  is increased so that decays of  $R$  into SM particles are additionally suppressed. Still, even for  $f_\chi^V = 1$ , we can exclude a direct detection cross-section above  $10^{-41} \text{ cm}^2$ , because larger mixing parameters are excluded by both dilepton and monojet constraints as well as EWPT.

## 5 Discussion

In this paper, we have considered a new vector state  $R$ , as the dominant mediator of the scattering between DM and nuclei, relevant for direct detection experiments. We have demonstrated that the LHC can significantly constrain the scattering cross-sections over a wide range of mediator masses. In the case of fermionic DM and assuming that the vector mediator has direct couplings to quarks, we can exclude cross-sections  $\sigma_p > 2 \times 10^{-40} \text{ cm}^2$  for  $300 \text{ GeV} \leq m_R \leq 1000 \text{ GeV}$  as long as  $m_\chi \ll m_R$ , with similar limits for scalar DM. When couplings to quarks are introduced only via mixing, the resulting bounds on the direct detection cross-section can be much stronger. However, it is possible to suppress the collider constraints by making the DM coupling very large compared to the quark couplings. Our approach allows a very general interpretation of the results from MET



searches at the LHC, because we have not assumed that the mediator is heavy enough for an effective operator analysis. Nevertheless, we have made other assumptions in our analysis, which we discuss below.

First, the DM particle has been assumed to have a mass  $m_\chi \ll m_R$ . When  $m_\chi$  becomes larger than  $m_R/2$ ,  $R$  can no longer decay into DM particles and therefore monojet signals can only arise when the mediator is produced off-shell. Hence bounds from monojets become much weaker. We do not consider this case further, as LHC bounds on the interactions of heavy DM are significantly less stringent than those obtained from direct detection experiments.

Second, we have assumed family independent fermion couplings (but we allow differences between up-quark and down-quark couplings, and between charged lepton and neutrino couplings). Coupling the mediator predominantly to the third generation would slightly relax the bound from dileptons, but make the already quite strong bound on top-quarks even stronger. At the same time, doing so would strongly suppress the direct detection cross-section. Consequently, allowing family-dependent couplings would not significantly change our conclusions.

Third, we have only considered the contribution from DY production of  $R$ . This is certainly justified in the case where couplings of  $R$  to standard model particles arise from kinetic mixing. For large  $m_R$ , however, the coupling of  $R$  to  $WW$  is not well constrained, so it could in general be possible to enhance the cross-section of VBF production. By neglecting additional contributions to the production of  $R$  we give of course a more conservative bound.

Fourth, there is only a relatively limited range of mediator masses, viz. 300–600 GeV, where we have bounds on all possible SM decay channels. Below 300 GeV, it will be difficult to constrain some of the couplings of  $R$  using LHC data, mostly because of QCD backgrounds. Instead, EWPT will become more important (see [33]). To extend the range of mediator masses above 600 GeV, we have simply assumed that the bound on  $\text{BR}(R \rightarrow WW)$  above 600 GeV is identical to that on  $\text{BR}(R \rightarrow ZZ)$ . Since the total width of the mediator is not very sensitive to this bound, we expect our result to be only mildly affected if the observed bound is significantly weaker.

Finally, and most importantly, we have assumed that we can treat  $R$  as a narrow resonance and we make extensive use of the NWA to separate the production of  $R$  from the subsequent decays. This factorisation is not valid for broad resonances, where we expect a significant contribution from off-shell mediators (see [45] for a discussion). Moreover, most bounds only apply for a narrow resonance. For example, limits for dijet resonances have only been published for peaks with  $\Gamma/M \lesssim 0.3$ .

We observe that for  $m_R < 1000$  GeV, present experimental results give the constraint  $\Gamma_R/m_R < 0.25$ . For these values, we expect the NWA to be accurate within a few percent. As  $m_R$  increases, the bounds on the individual coupling constants, and therefore the bound on  $\Gamma_R$ , become weaker. For  $m_R > 1$  TeV, couplings can be of order unity for which the width becomes so large that neither experimental limits nor the formalism presented in this paper can be applied. With increasing luminosity at the LHC, we expect to be able to extend our treatment to larger mediator masses, while at the same time obtaining stronger bounds on the direct detection cross-section.

For dark matter masses  $m_\chi \ll m_R$ , dark matter annihilation will only involve off-shell mediators. If the mediator couples mostly to quarks and dark matter, it is therefore possible to describe annihilation in terms of the same effective operators as direct detection. Consequently, one can directly translate between direct detection cross-sections and annihilation cross sections (see for example [67, 68]). In the case of a vector mediator and light dark matter, direct detection cross-sections of  $10^{-40} \text{ cm}^2$  or smaller correspond to an annihilation cross section significantly below the thermal cross section [14, 69].

The LHC bounds on the decay channels of  $R$  therefore imply that the annihilation cross section of dark matter into quarks is well below the present experimental sensitivity for dark matter indirect detection in all relevant channels including the antiproton flux from PAMELA [70], diffuse gamma rays from FERMI-LAT [71–73] and neutrinos from the sun [74].<sup>3</sup> Even more restrictive experimental bounds in the future can be evaded either if dark matter is asymmetric or by appealing to additional uncertainties as in [76, 77].

To obtain the required dark matter relic density in our framework, we must assume either the presence of additional mediators in the early universe in order to avoid overproduction of DM or additional couplings of  $R$  to new hidden sector states. In fact, coupling  $R$  to new hidden sector states that decay into SM particles with more complicated experimental signatures is an interesting possibility to evade experimental limits on  $\Gamma_R$ . Thus there are good reasons to carry out experimental searches (see [78] for an example) for such states.

## Acknowledgments

We thank Alan Barr, Georgios Choudalakis, James Unwin, Stephen West and Stephen Worm for helpful discussions. We have also benefitted from discussions with participants at the workshop on “*New Paths to Particle Dark Matter*” at Oxford, 28-29 April 2012. MTF is supported by an STFC grant, FK by the DAAD, and KSH by ERC Advanced Grant (BSMOXFORD 228169). We also acknowledge support from the UNILHC network (PITN-GA-2009-237920) and an IPPP associateship for 2011-12 awarded to SS.

## A Decay widths

$$\Gamma(R \rightarrow \chi\bar{\chi}) = \frac{m_R}{12\pi} \sqrt{1 - \frac{4m_\chi^2}{m_R^2}} [(g_\chi^V)^2 + (g_\chi^A)^2 + \frac{m_\chi^2}{m_R^2} (2(g_\chi^V)^2 - 4(g_\chi^A)^2)] \quad (\text{A.1})$$

$$\Gamma(R \rightarrow \phi\phi^*) = \frac{m_R}{48\pi} \sqrt{1 - \frac{4m_\phi^2}{m_R^2}} g_{R\phi}^2 \quad (\text{A.2})$$

$$\Gamma(R \rightarrow f\bar{f}) = \frac{m_R N_c}{12\pi} \sqrt{1 - \frac{4m_f^2}{m_R^2}} [(g_f^V)^2 + (g_f^A)^2 + \frac{m_f^2}{m_R^2} (2(g_f^V)^2 - 4(g_f^A)^2)] \quad (\text{A.3})$$

---

<sup>3</sup>However, if  $R$  has only small coupling to quarks, there could be a monoenergetic gamma ray signal from annihilation of dark matter into Z gamma as in [75].

$$\begin{aligned}
 \Gamma(R \rightarrow W^+ W^-) = & \frac{1}{192\pi} m_R \left( \frac{m_R}{m_W} \right)^4 \left( 1 - 4 \frac{m_W^2}{m_R^2} \right)^{1/2} \\
 & \left( (g_{WW1}^R)^2 \left[ 4 \frac{m_W^2}{m_R^2} - 4 \frac{m_W^4}{m_R^4} - 48 \frac{m_W^6}{m_R^6} \right] \right. \\
 & \quad + (g_{WW2}^R)^2 \left[ 1 - 16 \frac{m_W^4}{m_R^4} \right] \\
 & \quad + g_{WW1}^R g_{WW2}^R \left[ 12 \frac{m_W^2}{m_R^2} - 48 \frac{m_W^4}{m_R^4} \right] \\
 & \quad \left. + (g_{WW3}^R)^2 \left[ 4 \frac{m_W^2}{m_R^2} - 32 \frac{m_W^4}{m_R^4} + 64 \frac{m_W^6}{m_R^6} \right] \right) \quad (A.4)
 \end{aligned}$$

$$\Gamma(R \rightarrow ZZ) = \frac{(g_{ZZ}^R)^2}{96\pi} m_R \frac{m_R^2}{m_Z^2} \left( 1 - 4 \frac{m_Z^2}{m_R^2} \right)^{3/2} \left[ 1 - 6 \frac{m_Z^2}{m_R^2} \right] \quad (A.5)$$

$$\Gamma(R \rightarrow Z\gamma) = \frac{(g_{Z\gamma}^R)^2}{96\pi} m_R \frac{m_R^2}{m_Z^2} \left( 1 - \frac{m_Z^2}{m_R^2} \right)^3 \quad (A.6)$$

$$\Gamma(R \rightarrow ZH) = \frac{(g_{ZH}^R)^2}{192\pi m_Z^2} m_R \sqrt{\lambda(1, x_Z, x_H)} (\lambda(1, x_Z, x_H) + 12x_Z), \quad (A.7)$$

where  $x_Z = (m_Z/m_R)^2$ ,  $x_H = (m_H/m_R)^2$ , and  $\lambda(x, y, z) = x^2 + y^2 + z^2 - 2xy - 2yz - 2zx$ . Note that in the latter formula  $g_{ZH}^R$  has mass dimension one, following our conventions in the main text, and the expression agrees with that given in e.g. [79].

## B Coupling structure from mixing

In this appendix, we discuss how the mass eigenstate  $R$  arises from the mixing of an interaction eigenstate vector  $X$  with the SM  $U(1)_Y$   $B$  field and the neutral component  $W^3$  of  $SU(2)_L$  weak fields. We first consider the most general case and calculate the effective coupling constants defined in section 2 in terms of the fundamental couplings and the entries of the mixing matrix. We then calculate the mixing matrix that arises from kinetic mixing and mass mixing of gauge bosons.

Following the notation in [33] we write the general mixing matrix as

$$\begin{pmatrix} \hat{B}_\mu \\ \hat{W}_\mu^3 \\ \hat{X}_\mu \end{pmatrix} = \begin{pmatrix} N_{11} & N_{12} & N_{13} \\ N_{21} & N_{22} & N_{23} \\ N_{31} & N_{32} & N_{33} \end{pmatrix} \begin{pmatrix} A_\mu \\ Z_\mu \\ R_\mu \end{pmatrix}. \quad (B.1)$$

Here  $A$ ,  $Z$  are the physical photon and neutral massive gauge boson fields of the SM. The couplings of  $R$  to SM fermions are given in terms of the mass mixing matrix, as<sup>4</sup>

$$\begin{aligned}
 g_{uR}^V &= -\frac{1}{12}(5\hat{g}'N_{13} + 3\hat{g}N_{23}) - f_u^V N_{33}, & g_{uR}^A &= \frac{1}{4}(\hat{g}'N_{13} - \hat{g}N_{23}) - f_u^A N_{33}, \\
 g_{dR}^V &= \frac{1}{12}(\hat{g}'N_{13} + 3\hat{g}N_{23}) - f_d^V N_{33}, & g_{dR}^A &= -\frac{1}{4}(\hat{g}'N_{13} - \hat{g}N_{23}) - f_d^A N_{33},
 \end{aligned}$$

<sup>4</sup>We use  $\hat{g}$  and  $\hat{g}'$  to denote the fundamental gauge couplings of  $SU(2)_L$  and  $U(1)_Y$ , which will be different from the observed ones,  $g$  and  $g'$ .

$$\begin{aligned}
 g_{eR}^V &= \frac{1}{4}(3\hat{g}'N_{13} + \hat{g}N_{23}) - f_e^V N_{33}, & g_{eR}^A &= -\frac{1}{4}(\hat{g}'N_{13} - \hat{g}N_{23}) - f_e^A N_{33}, \\
 g_{\nu R}^V &= \frac{1}{4}(\hat{g}'N_{13} - \hat{g}N_{23}) - f_\nu^V N_{33}, & g_{\nu R}^A &= -\frac{1}{4}(\hat{g}'N_{13} - \hat{g}N_{23}) - f_\nu^A N_{33},
 \end{aligned} \quad (B.2)$$

where the numerical coefficients are determined from the hypercharge and weak quantum numbers of the SM fermions and  $f^{V,A}$  denote the direct couplings of  $X$ . Similarly, the effective vector and axial couplings of  $R$  to the DM particle are given by

$$g_{\chi R}^V = f_\chi^V N_{33}, \quad g_{\chi R}^A = f_\chi^A N_{33} \quad \text{or} \quad g_{\phi R} = f_\phi N_{33} \quad (B.3)$$

depending on whether the DM particle is a fermion or a scalar.

Finally, the couplings of  $R$  to SM bosons are given by [28]

$$\begin{aligned}
 g_{WW1}^R &= g_{WW2}^R = \hat{g}N_{23}, & g_{ZWW1}^R &= -\hat{g}^2 N_{22}N_{23}, & g_{AWW1}^R &= -\hat{g}^2 N_{21}N_{23}, \\
 g_{ZH}^R &= \frac{v}{2}(\hat{g}'N_{12} - \hat{g}N_{22})(\hat{g}'N_{13} - \hat{g}N_{23}), & g_{HH}^R &= \frac{1}{2}(\hat{g}'N_{12} - \hat{g}N_{22})(\hat{g}'N_{13} - \hat{g}N_{23}).
 \end{aligned} \quad (B.4)$$

(B.5)

Since  $P$ -violating couplings of gauge bosons are absent in the SM, the corresponding couplings of  $R$  cannot be introduced by mixing alone.

We now assume that  $X$  is the gauge boson of a new  $U(1)_X$  gauge group and follow the discussion in [33] of an effective Lagrangian which includes kinetic mixing and mass mixing (see also [23])

$$\begin{aligned}
 \mathcal{L} &= \mathcal{L}_{SM} - \frac{1}{4}\hat{X}^{\mu\nu}\hat{X}_{\mu\nu} + \frac{1}{2}m_X^2\hat{X}_\mu\hat{X}^\mu - m_\chi\bar{\chi}\chi \\
 &\quad - \frac{1}{2}\sin\epsilon\hat{B}_{\mu\nu}\hat{X}^{\mu\nu} + \delta m^2\hat{Z}_\mu\hat{X}^\mu - \sum_f f_f^V\hat{X}^\mu\bar{f}\gamma_\mu f - f_\chi^V\hat{X}^\mu\bar{\chi}\gamma_\mu\chi.
 \end{aligned} \quad (B.6)$$

As in [38], we assume that the  $U(1)_X$  is broken by an additional Higgs field and  $X$  acquires the mass  $m_X$ . We will not discuss the implications of this additional Higgs field and its potential mixing further. We define  $\hat{Z} \equiv \hat{c}_W\hat{W}^3 - \hat{s}_W\hat{B}$ , where  $\hat{s}_W$  ( $\hat{c}_W$ ) is the sine (cosine) of the (fundamental) Weinberg angle.

The diagonalisation of the above Lagrangian is discussed in detail in e.g. [23]. The field strengths are diagonalised and canonically normalised via the following two consecutive transformations

$$\begin{pmatrix} \hat{B}_\mu \\ \hat{W}_\mu^3 \\ \hat{X}_\mu \end{pmatrix} = \begin{pmatrix} 1 & 0 & -t_\epsilon \\ 0 & 1 & 0 \\ 0 & 0 & 1/c_\epsilon \end{pmatrix} \begin{pmatrix} B_\mu \\ W_\mu^3 \\ X_\mu \end{pmatrix}, \quad (B.7)$$

$$\begin{pmatrix} B_\mu \\ W_\mu^3 \\ X_\mu \end{pmatrix} = \begin{pmatrix} \hat{c}_W & -\hat{s}_W c_\xi & \hat{s}_W s_\xi \\ \hat{s}_W & \hat{c}_W c_\xi & -\hat{c}_W s_\xi \\ 0 & s_\xi & c_\xi \end{pmatrix} \begin{pmatrix} A_\mu \\ Z_\mu \\ R_\mu \end{pmatrix}, \quad (B.8)$$

where

$$t_{2\xi} = \frac{-2c_\epsilon(\delta m^2 + m_Z^2\hat{s}_W s_\epsilon)}{m_X^2 - m_Z^2 c_\epsilon^2 + m_Z^2\hat{s}_W^2 s_\epsilon^2 + 2\delta m^2\hat{s}_W s_\epsilon}. \quad (B.9)$$

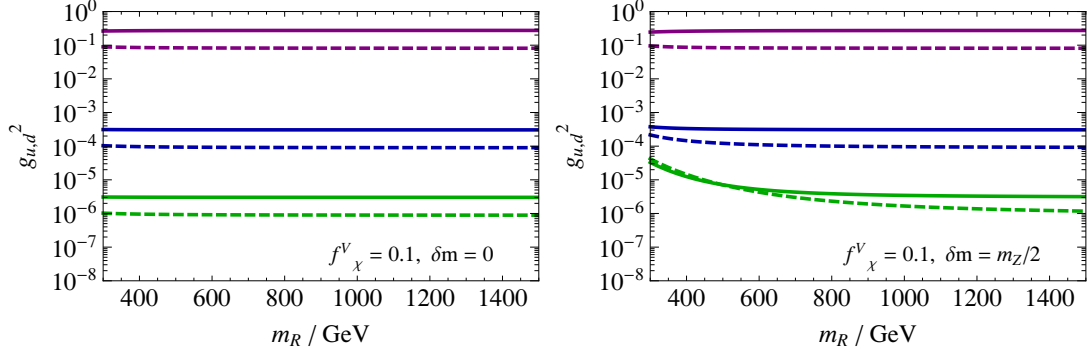


**Figure 18.** The couplings  $g_u^2$  (solid lines) and  $g_d^2$  (dashed lines) as a function of  $m_R$  for  $\epsilon = 0.01$  (green),  $\epsilon = 0.1$  (blue) and  $\epsilon = 1$  (purple). In the left plot, interactions are induced by kinetic mixing only via the Lagrangian given in equation (B.6), while in the right plot we have included a mass mixing of  $\delta m = m_Z/2$ .

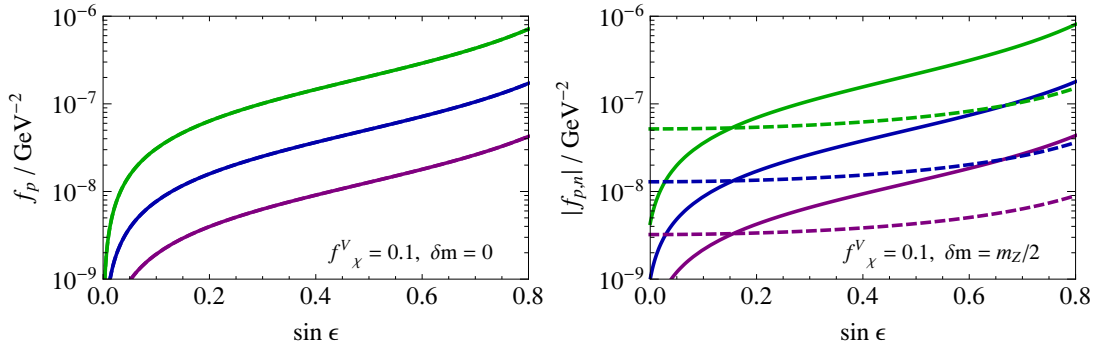


**Figure 19.** The effective couplings  $f_p$  (solid lines) and  $f_n$  (dashed lines) obtained from the Lagrangian given in equation (B.6) as a function of  $\sin \epsilon$  for  $m_R = 300$  GeV (green),  $m_R = 600$  GeV (blue) and  $m_R = 1200$  GeV (purple). In the left plot, interactions are induced by kinetic mixing only, so  $f_n = 0$ , while in the right plot we have included a mass mixing of  $\delta m = m_Z/2$ .

Multiplying the two matrices, we obtain the coefficients  $N_{ij}$  so that we can calculate the couplings of  $R$  using equations (B.2)–(B.5). As discussed in [28, 33], the fundamental parameters  $m_{\hat{Z}}$  and  $\hat{s}_W$  are constrained by the requirement that the physical  $Z$  mass and the Weinberg angle come out in accord with experiment.

At colliders we are directly sensitive to the couplings  $g_{u,d}$ , which determine the production cross-section of  $R$  (see section 2.2). We show these in figure 18 as a function of  $m_R$  for different values of the kinetic mixing parameter  $\epsilon$  and different values of the mass mixing parameter  $\delta m$ .

If there are no direct couplings to quarks, we can calculate the effective DM-nucleon couplings  $f_p$  and  $f_n$  in terms of  $\epsilon$ ,  $\delta m$  and  $f_\chi^V$ , cf. equation (4.10). We show these couplings as a function of  $\sin \epsilon$  for different values of  $\delta m$  in figure 19. Note that for  $\delta m = 0$ , we obtain  $f_n/f_p = 0$ , while for  $\delta m \neq 0$ ,  $f_n/f_p < 0$ .

## References

- [1] XENON100 collaboration, E. Aprile et al., *Dark matter results from 100 live days of XENON100 data*, *Phys. Rev. Lett.* **107** (2011) 131302 [[arXiv:1104.2549](#)] [[INSPIRE](#)].
- [2] CDMS-II collaboration, Z. Ahmed et al., *Dark matter search results from the CDMS II experiment*, *Science* **327** (2010) 1619 [[arXiv:0912.3592](#)] [[INSPIRE](#)].
- [3] CDMS-II collaboration, Z. Ahmed et al., *Results from a low-energy analysis of the CDMS II germanium data*, *Phys. Rev. Lett.* **106** (2011) 131302 [[arXiv:1011.2482](#)] [[INSPIRE](#)].
- [4] DAMA, LIBRA collaboration, R. Bernabei et al., *New results from DAMA/LIBRA*, *Eur. Phys. J. C* **67** (2010) 39 [[arXiv:1002.1028](#)] [[INSPIRE](#)].
- [5] C. Aalseth et al., *Search for an annual modulation in a P-type point contact germanium dark matter detector*, *Phys. Rev. Lett.* **107** (2011) 141301 [[arXiv:1106.0650](#)] [[INSPIRE](#)].
- [6] G. Angloher et al., *Results from 730 kg days of the CRESST-II dark matter search*, *Eur. Phys. J. C* **72** (2012) 1971 [[arXiv:1109.0702](#)] [[INSPIRE](#)].
- [7] DELPHI collaboration, J. Abdallah et al., *Photon events with missing energy in  $e^+e^-$  collisions at  $\sqrt{s} = 130 \text{ GeV}$  to  $209 \text{ GeV}$* , *Eur. Phys. J. C* **38** (2005) 395 [[hep-ex/0406019](#)] [[INSPIRE](#)].
- [8] CDF collaboration, *Search for extra dimensions in jets+missing energy in RunII*, <http://www-cdf.fnal.gov/physics/exotic/r2a/20070322.monojet/public/ykk.html> (2007).
- [9] CMS collaboration, *Search for new physics with a monojet and missing transverse energy in pp collisions at  $\sqrt{s} = 7 \text{ TeV}$* , *PAS-EXO-11-059* (2011).
- [10] ATLAS collaboration, G. Aad et al., *Search for new phenomena in  $t\bar{t}$  events with large missing transverse momentum in proton-proton collisions at  $\sqrt{s} = 7 \text{ TeV}$  with the ATLAS detector*, *Phys. Rev. Lett.* **108** (2012) 041805 [[arXiv:1109.4725](#)] [[INSPIRE](#)].
- [11] CMS collaboration, *Search for ADD extra-dimensions in monophotons*, *PAS-EXO-11-058* (2011).
- [12] CMS collaboration, S. Chatrchyan et al., *Search for dark matter and large extra dimensions in pp collisions yielding a photon and missing transverse energy*, [arXiv:1204.0821](#) [[INSPIRE](#)].
- [13] J. Goodman et al., *Constraints on light majorana dark matter from colliders*, *Phys. Lett. B* **695** (2011) 185 [[arXiv:1005.1286](#)] [[INSPIRE](#)].
- [14] Y. Bai, P.J. Fox and R. Harnik, *The Tevatron at the frontier of dark matter direct detection*, *JHEP* **12** (2010) 048 [[arXiv:1005.3797](#)] [[INSPIRE](#)].
- [15] A. Rajaraman, W. Shepherd, T.M. Tait and A.M. Wijangco, *LHC bounds on interactions of dark matter*, *Phys. Rev. D* **84** (2011) 095013 [[arXiv:1108.1196](#)] [[INSPIRE](#)].
- [16] J. Goodman et al., *Constraints on dark matter from colliders*, *Phys. Rev. D* **82** (2010) 116010 [[arXiv:1008.1783](#)] [[INSPIRE](#)].
- [17] P.J. Fox, R. Harnik, J. Kopp and Y. Tsai, *LEP shines light on dark matter*, *Phys. Rev. D* **84** (2011) 014028 [[arXiv:1103.0240](#)] [[INSPIRE](#)].
- [18] P.J. Fox, R. Harnik, J. Kopp and Y. Tsai, *Missing energy signatures of dark matter at the LHC*, *Phys. Rev. D* **85** (2012) 056011 [[arXiv:1109.4398](#)] [[INSPIRE](#)].

- [19] I.M. Shoemaker and L. Vecchi, *Unitarity and monojet bounds on models for DAMA, CoGeNT and CRESST-II*, [arXiv:1112.5457](#) [INSPIRE].
- [20] P.J. Fox, R. Harnik, R. Primulando and C.-T. Yu, *Taking a razor to dark matter parameter space at the LHC*, [arXiv:1203.1662](#) [INSPIRE].
- [21] J. March-Russell, J. Unwin and S.M. West, *Closing in on asymmetric dark matter I: model independent limits for interactions with quarks*, [arXiv:1203.4854](#) [INSPIRE].
- [22] B. Holdom, *Two U(1)'s and  $\epsilon$  charge shifts*, *Phys. Lett. B* **166** (1986) 196 [INSPIRE].
- [23] K. Babu, C.F. Kolda and J. March-Russell, *Implications of generalized Z-Z' mixing*, *Phys. Rev. D* **57** (1998) 6788 [[hep-ph/9710441](#)] [INSPIRE].
- [24] S. Cassel, D. Ghilencea and G. Ross, *Electroweak and dark matter constraints on a Z' in models with a hidden valley*, *Nucl. Phys. B* **827** (2010) 256 [[arXiv:0903.1118](#)] [INSPIRE].
- [25] A. Hook, E. Izaguirre and J.G. Wacker, *Model independent bounds on kinetic mixing*, *Adv. High Energy Phys.* **2011** (2011) 859762 [[arXiv:1006.0973](#)] [INSPIRE].
- [26] Y. Mambrini, *The Kinetic dark-mixing in the light of CoGENT and XENON100*, *JCAP* **09** (2010) 022 [[arXiv:1006.3318](#)] [INSPIRE].
- [27] Z. Kang, T. Li, T. Liu, C. Tong and J.M. Yang, *Light dark matter from the U(1)<sub>X</sub> sector in the NMSSM with gauge mediation*, *JCAP* **01** (2011) 028 [[arXiv:1008.5243](#)] [INSPIRE].
- [28] E.J. Chun, J.-C. Park and S. Scopel, *Dark matter and a new gauge boson through kinetic mixing*, *JHEP* **02** (2011) 100 [[arXiv:1011.3300](#)] [INSPIRE].
- [29] P.J. Fox, J. Liu, D. Tucker-Smith and N. Weiner, *An effective Z'*, *Phys. Rev. D* **84** (2011) 115006 [[arXiv:1104.4127](#)] [INSPIRE].
- [30] Y. Mambrini, *The ZZ' kinetic mixing in the light of the recent direct and indirect dark matter searches*, *JCAP* **07** (2011) 009 [[arXiv:1104.4799](#)] [INSPIRE].
- [31] P. Gondolo, P. Ko and Y. Omura, *Light dark matter in leptophobic Z' models*, *Phys. Rev. D* **85** (2012) 035022 [[arXiv:1106.0885](#)] [INSPIRE].
- [32] Y. Mambrini and B. Zaldivar, *When LEP and Tevatron combined with WMAP and XENON100 shed light on the nature of dark matter*, *JCAP* **10** (2011) 023 [[arXiv:1106.4819](#)] [INSPIRE].
- [33] M.T. Frandsen, F. Kahlhoefer, S. Sarkar and K. Schmidt-Hoberg, *Direct detection of dark matter in models with a light Z'*, *JHEP* **09** (2011) 128 [[arXiv:1107.2118](#)] [INSPIRE].
- [34] J.M. Cline and A.R. Frey, *Minimal hidden sector models for CoGeNT/DAMA events*, *Phys. Rev. D* **84** (2011) 075003 [[arXiv:1108.1391](#)] [INSPIRE].
- [35] J. Heeck and W. Rodejohann, *Kinetic and mass mixing with three abelian groups*, *Phys. Lett. B* **705** (2011) 369 [[arXiv:1109.1508](#)] [INSPIRE].
- [36] R. Foadi, M.T. Frandsen and F. Sannino, *Technicolor dark matter*, *Phys. Rev. D* **80** (2009) 037702 [[arXiv:0812.3406](#)] [INSPIRE].
- [37] R. Barbieri, S. Rychkov and R. Torre, *Signals of composite electroweak-neutral dark matter: LHC/direct detection interplay*, *Phys. Lett. B* **688** (2010) 212 [[arXiv:1001.3149](#)] [INSPIRE].
- [38] E. Weihs and J. Zurita, *Dark Higgs models at the 7 TeV LHC*, *JHEP* **02** (2012) 041 [[arXiv:1110.5909](#)] [INSPIRE].



- [39] H. An, X. Ji and L.-T. Wang, *Light dark matter and  $Z'$  dark force at colliders*, [arXiv:1202.2894](#) [[INSPIRE](#)].
- [40] E. Del Nobile and F. Sannino, *Dark matter effective theory*, *Int. J. Mod. Phys. A* **27** (2012) 1250065 [[arXiv:1102.3116](#)] [[INSPIRE](#)].
- [41] K. Hagiwara, R. Peccei, D. Zeppenfeld and K. Hikasa, *Probing the weak boson sector in  $e^+e^- \rightarrow W^+W^-$* , *Nucl. Phys. B* **282** (1987) 253 [[INSPIRE](#)].
- [42] W.-Y. Keung, I. Low and J. Shu, *Landau-Yang theorem and decays of a  $Z'$  boson into two  $Z$  bosons*, *Phys. Rev. Lett.* **101** (2008) 091802 [[arXiv:0806.2864](#)] [[INSPIRE](#)].
- [43] T.G. Rizzo and R.W. Robinett, *Triple gauge boson decay of new neutral gauge bosons*, *Phys. Lett. B* **226** (1989) 117 [[INSPIRE](#)].
- [44] M.S. Carena, A. Daleo, B.A. Dobrescu and T.M. Tait,  *$Z'$  gauge bosons at the Tevatron*, *Phys. Rev. D* **70** (2004) 093009 [[hep-ph/0408098](#)] [[INSPIRE](#)].
- [45] E. Accomando, A. Belyaev, L. Fedeli, S.F. King and C. Shepherd-Themistocleous,  *$Z'$  physics with early LHC data*, *Phys. Rev. D* **83** (2011) 075012 [[arXiv:1010.6058](#)] [[INSPIRE](#)].
- [46] M.J. Strassler and K.M. Zurek, *Echoes of a hidden valley at hadron colliders*, *Phys. Lett. B* **651** (2007) 374 [[hep-ph/0604261](#)] [[INSPIRE](#)].
- [47] ATLAS collaboration, G. Aad et al., *Search for New physics in the dijet mass distribution using  $1 \text{ fb}^{-1}$  of  $pp$  collision data at  $\sqrt{s} = 7 \text{ TeV}$  collected by the ATLAS detector*, *Phys. Lett. B* **708** (2012) 37 [[arXiv:1108.6311](#)] [[INSPIRE](#)].
- [48] CDF collaboration, T. Aaltonen et al., *Search for new particles decaying into dijets in proton-antiproton collisions at  $\sqrt{s} = 1.96 \text{ TeV}$* , *Phys. Rev. D* **79** (2009) 112002 [[arXiv:0812.4036](#)] [[INSPIRE](#)].
- [49] CMS collaboration, *Search for resonances in the dilepton mass distribution in  $pp$  Collisions at  $\sqrt{s} = 7 \text{ TeV}$* , [PAS-EXO-11-019](#) (2011).
- [50] ATLAS collaboration, G. Aad et al., *Search for dilepton resonances in  $pp$  collisions at  $\sqrt{s} = 7 \text{ TeV}$  with the ATLAS detector*, *Phys. Rev. Lett.* **107** (2011) 272002 [[arXiv:1108.1582](#)] [[INSPIRE](#)].
- [51] CMS collaboration, *Search for high-mass resonances decaying into  $\tau$ -lepton pairs in  $pp$  collisions at  $\sqrt{s} = 7 \text{ TeV}$* , [CMS-PAS-EXO-11-031](#) (2012).
- [52] ATLAS collaboration, *An update to the combined search for the standard model Higgs boson with the ATLAS detector at the LHC using up to  $4.9 \text{ fb}^{-1}$  of  $pp$  collision data at  $\sqrt{s} = 7 \text{ TeV}$* , [ATLAS-CONF-2012-019](#) (2012).
- [53] ATLAS collaboration, G. Aad et al., *Search for new particles decaying to  $ZZ$  using final states with leptons and jets with the ATLAS detector in  $\sqrt{s} = 7 \text{ TeV}$  proton-proton collisions*, *Phys. Lett. B* **712** (2012) 331 [[arXiv:1203.0718](#)] [[INSPIRE](#)].
- [54] CMS collaboration, S. Chatrchyan et al., *Combined results of searches for the standard model Higgs boson in  $pp$  collisions at  $\sqrt{s} = 7 \text{ TeV}$* , *Phys. Lett. B* **710** (2012) 26 [[arXiv:1202.1488](#)] [[INSPIRE](#)].
- [55] ATLAS collaboration, *Search for the standard model Higgs boson produced in association with a vector boson and decaying to a  $b$ -quark pair using up to  $4.7 \text{ fb}^{-1}$  of  $pp$  collision data at  $\sqrt{s} = 7 \text{ TeV}$  with the ATLAS detector at the LHC*, [ATLAS-CONF-2012-015](#) (2012).



- [56] CMS collaboration, *Search for BSM  $t\bar{t}$  production in the boosted all-hadronic final state*, [PAS-EXO-11-006](#) (2011).
- [57] CMS collaboration, *A search for resonances in semileptonic top pair production*, [PAS-TOP-11-009](#) (2011).
- [58] D0 collaboration, V. Abazov et al., *Search for large extra dimensions in the monojet + missing  $E_T$  channel at  $D\bar{D}$* , *Phys. Rev. Lett.* **90** (2003) 251802 [[hep-ex/0302014](#)] [[INSPIRE](#)].
- [59] ATLAS collaboration, *Search for new phenomena in monojet plus missing transverse momentum final states using  $1\text{ fb}^{-1}$  of  $pp$  collisions at  $\sqrt{s} = 7\text{ TeV}$  with the ATLAS Detector*, [ATLAS-CONF-2011-096](#) (2011).
- [60] A. Pukhov, *CalcHEP 2.3: MSSM, structure functions, event generation, batchs and generation of matrix elements for other packages*, [hep-ph/0412191](#) [[INSPIRE](#)].
- [61] G. Choudalakis, *How to use experimental data to compute the probability of your theory*, [arXiv:1110.5295](#) [[INSPIRE](#)].
- [62] A. Semenov, *LanHEP — A package for automatic generation of Feynman rules from the Lagrangian. Updated version 3.1*, [arXiv:1005.1909](#) [[INSPIRE](#)].
- [63] LEP WORKING GROUP FOR HIGGS BOSON SEARCHES, ALEPH, DELPHI, L3, OPAL collaboration, R. Barate et al., *Search for the standard model Higgs boson at LEP*, *Phys. Lett. B* **565** (2003) 61 [[hep-ex/0306033](#)] [[INSPIRE](#)].
- [64] M.T. Frandsen et al., *On the DAMA and CoGeNT modulations*, *Phys. Rev. D* **84** (2011) 041301 [[arXiv:1105.3734](#)] [[INSPIRE](#)].
- [65] S.B. Gudnason, C. Kouvaris and F. Sannino, *Dark matter from new technicolor theories*, *Phys. Rev. D* **74** (2006) 095008 [[hep-ph/0608055](#)] [[INSPIRE](#)].
- [66] M.T. Frandsen, S. Sarkar and K. Schmidt-Hoberg, *Light asymmetric dark matter from new strong dynamics*, *Phys. Rev. D* **84** (2011) 051703 [[arXiv:1103.4350](#)] [[INSPIRE](#)].
- [67] J.-M. Zheng et al., *Constraining the interaction strength between dark matter and visible matter: I. fermionic dark matter*, *Nucl. Phys. B* **854** (2012) 350 [[arXiv:1012.2022](#)] [[INSPIRE](#)].
- [68] K. Cheung, P.-Y. Tseng and T.-C. Yuan, *Gamma-ray constraints on effective interactions of the dark matter*, *JCAP* **06** (2011) 023 [[arXiv:1104.5329](#)] [[INSPIRE](#)].
- [69] M. Beltrán, D. Hooper, E.W. Kolb and Z.C. Krusberg, *Deducing the nature of dark matter from direct and indirect detection experiments in the absence of collider signatures of new physics*, *Phys. Rev. D* **80** (2009) 043509 [[arXiv:0808.3384](#)] [[INSPIRE](#)].
- [70] PAMELA collaboration, O. Adriani et al., *PAMELA results on the cosmic-ray antiproton flux from 60 MeV to 180 GeV in kinetic energy*, *Phys. Rev. Lett.* **105** (2010) 121101 [[arXiv:1007.0821](#)] [[INSPIRE](#)].
- [71] FERMI-LAT collaboration, M. Ackermann et al., *Constraining dark matter models from a combined analysis of Milky Way satellites with the Fermi Large Area Telescope*, *Phys. Rev. Lett.* **107** (2011) 241302 [[arXiv:1108.3546](#)] [[INSPIRE](#)].
- [72] A. Geringer-Sameth and S.M. Koushiappas, *Exclusion of canonical WIMPs by the joint analysis of Milky Way dwarfs with Fermi*, *Phys. Rev. Lett.* **107** (2011) 241303 [[arXiv:1108.2914](#)] [[INSPIRE](#)].

- [73] M. Mazziotta, F. Loparco, F. de Palma and N. Giglietto, *A model-independent analysis of the Fermi Large Area Telescope  $\gamma$ -ray data from the Milky Way dwarf galaxies and halo to constrain dark matter scenarios*, [arXiv:1203.6731](#) [[INSPIRE](#)].
- [74] R. Kappl and M.W. Winkler, *New limits on dark matter from Super-Kamiokande*, *Nucl. Phys. B* **850** (2011) 505 [[arXiv:1104.0679](#)] [[INSPIRE](#)].
- [75] E. Dudas, Y. Mambrini, S. Pokorski and A. Romagnoni, *(In)visible  $Z'$  and dark matter*, *JHEP* **08** (2009) 014 [[arXiv:0904.1745](#)] [[INSPIRE](#)].
- [76] A. Charbonnier et al., *Dark matter profiles and annihilation in dwarf spheroidal galaxies: perspectives for present and future gamma-ray observatories — I. The classical dSphs*, *Mon. Not. Roy. Astron. Soc.* **418** (2011) 1526 [[arXiv:1104.0412](#)] [[INSPIRE](#)].
- [77] I. Cholis and P. Salucci, *Extracting limits on dark matter annihilation from dwarf spheroidal galaxies at  $\gamma$ -rays*, [arXiv:1203.2954](#) [[INSPIRE](#)].
- [78] ATLAS collaboration, G. Aad et al., *Search for a light Higgs boson decaying to long-lived weakly-interacting particles in proton-proton collisions at  $\sqrt{s} = 7$  TeV with the ATLAS detector*, *Phys. Rev. Lett.* **108** (2012) 251801 [[arXiv:1203.1303](#)] [[INSPIRE](#)].
- [79] V. Barger, P. Langacker and H.-S. Lee, *Six-lepton  $Z'$  resonance at the LHC*, *Phys. Rev. Lett.* **103** (2009) 251802 [[arXiv:0909.2641](#)] [[INSPIRE](#)].